Control amplitude and phase of light by plasmonic meta-hologram with T-shaped nano-cavity

Wei Song (宋 伟), Shanguang Zheng (郑闪光), Yanan Fu (付亚男), Changjun Min (闵长俊)*, Yuquan Zhang (张聿全), Zhenwei Xie (谢振威), and Xiaocong Yuan (袁小聪)**

Nanophotonics Research Center, Shenzhen Key Laboratory of Micro-Scale Optical Information Technology, Shenzhen University, Shenzhen 518060, China

**Corresponding author: cjmin@szu.edu.cn; **corresponding author: xcyuan@szu.edu.cn*

Received January 16, 2019; accepted March 13, 2019; posted online May 31, 2019

Controlling both amplitude and phase of light in the subwavelength scale is a challenge for traditional optical devices. Here, we propose and numerically investigate a novel plasmonic meta-hologram, demonstrating broadband manipulation of both phase and amplitude in the subwavelength scale. In the meta-hologram, phase modulation is achieved by the detour phase distribution of unit cells, and amplitude is continuously modulated by a T-shaped nano-cavity with tunable plasmonic resonance. Compared to phase-only holograms, such a meta-hologram could reconstruct three-dimensional (3D) images with higher signal-to-noise ratio and better image quality, thus offering great potential in applications such as 3D displays, optical communications, and beam shaping.

OCIS codes: 240.6680, 160.3918, 090.2890.
doi: 10.3788/COL201917.062402.

Holography is a very powerful technology for recording and reconstructing three-dimensional (3D) optical information of the target object in free space and is widely used in various optical fields, including 3D imaging, optical storage, optical communication, and others[1–3]. Traditional holographic imaging technology is generally achieved by common optical devices, such as a spatial light modulator or digital micromirror device. These devices have pixel sizes much larger than the working wavelength and, thus, suffer from drawbacks, such as low spatial resolution, narrow viewing angle, large device size, and unnecessary twin image[3]. Besides, these devices could only modulate a single parameter of light (amplitude, phase, or polarization), while the simultaneous control of multiple parameters of light for holography is still a challenge.

Recently, thanks to the rapid development of nanofabrication techniques, a variety of subwavelength optical devices have been proposed and studied, showing advantages of ultra-compact size and novel functions for optical modulation, which offer great potential in breaking through the limitation of traditional devices for 3D holographic imaging[4–6]. As a new type of subwavelength devices, the metasurface has attracted enormous interest for the fantastic capability of tailoring the wavefront of light at the nanoscale by engineering the optical resonance or geometric orientation[7–9] of optical scatterers (or optical antennas)[10], such as metallic nanorods[11] and V-shaped nano-antennas[12]. Numerous metasurfaces have been proposed to realize the arbitrary phase profile of light from the visible to terahertz wave bands[13] and, consequently, contribute to diverse applications, including ultrathin meta-lens[14,15], orbital angular momentum modulation[16–18], photonic spin Hall effect detection[19], active-controlled devices[20], and chiral-dependent multifunctional devices[21,22]. Metasurface-based hologram devices (called meta-holograms) have also been investigated in recent years[5,11,21–23]. However, many previous meta-holograms were designed for pure phase modulation rather than complex amplitude modulation and, thus, had to work with a phase retrieval algorithm[5,23] that is time-consuming and could degrade the performance of 3D holographic imaging[24]. Attempts have been made to manipulate both the amplitude and phase of light in recent years, but some previous works are limited by the only two- or four-level amplitude modulation capability[25,26].

In our previous works, we proposed a phase-only meta-hologram based on a plasmonic nano-slits array[27] and then achieved complex amplitude modulation by inserting multiple nano-slits in each unit cell of the meta-hologram[28]. However, such an amplitude modulation method suffers from the limited number of nano-slits and the discrete adjustment of amplitude. Besides, the coupling effect between adjacent nano-slits could influence the accuracy in amplitude and phase manipulation.

In this Letter, we propose and numerically study a new plasmonic meta-hologram based on a T-shaped nano-cavity and detour phase, showing advantages of continuous amplitude and phase modulation for 3D holographic imaging. In the T-shaped nano-cavity, the amplitude of transmitted light is strongly dependent on the resonance of surface plasmon polaritons (SPPs) inside the cavity; hence, we can modify the cavity structure to control the resonance as well as the transmittance amplitude. Our results show that the amplitude can either be enhanced or suppressed by adjusting the cavity structure parameters for continuous amplitude modulation. To realize a phase

modulation of 0–2π, the position of the T-shaped nano-cavity in each unit cell is determined by the detour phase principle. With combination of the T-shaped nano-cavity and detour phase, we finally achieve the complete amplitude and phase control of light. To demonstrate the ability of the meta-hologram, we use it to reconstruct the 3D optical field in the broadband wavelength range by finite difference time domain (FDTD) simulations, showing good agreement with theoretical prediction. We also compare it with the phase-only meta-hologram and prove that such a device could reconstruct 3D images with higher signal-to-noise ratio (SNR) and better image quality.

Figure 1 shows the schematic of the proposed meta-hologram. The mechanism of detour phase used in the meta-hologram for phase modulation is shown in Fig. 1(a). Here, the meta-hologram is designed with a gold film etched with T-shaped nano-slits. The incident light is considered as a p-polarized plane wave with normal incidence from the bottom, which could excite SPPs passing through the T-shaped nano-slits and scattering to the far field. As indicated in Fig. 1(a), the scattered light beams from the two adjacent slits in the metal film act as two parallel line sources with equal phase and generate an optical path difference $\Delta L = D\sin\theta$ at the output angle θ. The corresponding phase difference is $\Delta\varphi = 2\pi\Delta L/\lambda = 2\pi D\sin\theta/\lambda$,

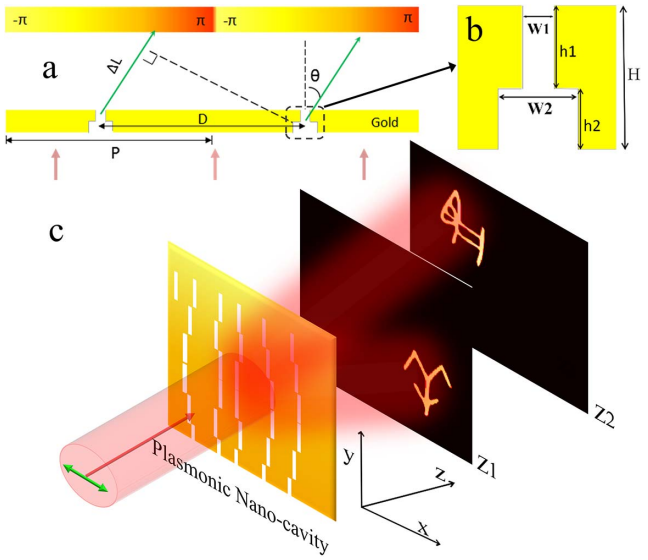

Fig. 1. Schematic of the structural design of the meta-hologram. a, Phase control of two adjacent unit cells with distance D. The cell is composed of a T-shaped nano-cavity in a gold film on a glass substrate. P denotes the period length of a single cell. The two cells induce an optical path difference ΔL at the output angle $\theta = \arcsin(\lambda/P)$. Each nano-cavity at different locations in period length P produces different phases (between $-\pi$ and π). b, Profile of the T-shaped nano-cavity. Gold film thickness is $H = 200$ nm, and the upper groove width is $w_1 = 50$ nm. The width w_2 and the height h_2 of the lower cavity are changed to control the transmittance amplitude. c, Typical 3D object reconstructed from the meta-hologram. When the meta-hologram is illuminated by a p-polarized light, the output beam generates the desired 3D object in free space.

depending on the distance D between adjacent slits, and thus, the phase difference $\Delta\varphi$ can be modulated from 0 to 2π by selecting the proper value of D. Then, we extend the two slits to a two-dimensional slit array with a period length $P = \lambda/\sin\theta$ for each unit cell. The output light from the slits with the same position in the unit cell should be in-phase ($\Delta\varphi = 2\pi P\sin\theta/\lambda = 2\pi$), while the light from the slits with different positions in the cell results in the phase difference $\Delta\varphi$ in the range of 0–2π, just as the conception of the detour phase[29,30]. That is, we can form a desired two-dimensional phase distribution $\varphi_{(i,j)}$ through the slit array by selecting all of the slit positions in each unit cell. In our design, we define the central position of the unit cell as $\varphi_{(i,j)} = 0$, and then we could get $\varphi_{(i,j)}$ changing from $-\pi$ to π when the slit location changes from the left to the right border of cell, just as is shown in the top of Fig. 1(a).

It is noted that, once the period length P is chosen, the output angle of light would be fixed as $\theta = \arcsin(\lambda/P)$, and the operation wavelength of the meta-hologram could be in the range from 0 to P when θ varies from 0° to 90°. Here, we choose the period length $P = 1$ μm in all calculations, and therefore, in theory, the meta-hologram could work with a broad band of wavelength from 0 to 1000 nm.

The amplitude modulation in the meta-hologram is achieved by adjusting the structure parameters of the T-shaped nano-slit. The detailed structure of the T-shaped nano-slit is shown in Fig. 1(b). Here, we choose the fixed gold film thickness $H = 200$ nm and the upper groove width $w_1 = 50$ nm according to the experimental parameters in our previous work[27], while the width w_2 and the height h_2 of the lower cavity are changed for the amplitude modulation. When a p-polarized light illuminates onto the T-shaped slit from the bottom, SPPs are firstly excited in the lower cavity, and then form a Fabry–Perot-like resonance inside the cavity. Since the SPP's resonant state is sensitive to the cavity structure, we can modulate such SPP resonance by adjusting the cavity width w_2 and height h_2 and subsequently control the amplitude of light passing through the slit. It is noted that, although directly increasing the slit width (w_1 and w_2) can also enhance the transmittance for amplitude modulation, however, it would greatly reduce the polarization extinction ratio (between p and s polarizations) in such plasmonic devices and influence the accuracy of the phase profile; hence, it is not a good choice. Here, the upper groove width is fixed at $w_1 = 50$ nm to keep a high polarization extinction ratio, and thereby such a device could still maintain the polarization multiplexing function as in our previous work[27].

Figure 1(c) shows the schematic of 3D object reconstruction through the meta-hologram. When the meta-hologram is illuminated with a p-polarized light, two Chinese oracle characters ("sheep" and "rabbit") are designed to be reconstructed at two different planes along the z axis. To achieve such reconstruction, we need to obtain the whole information of amplitude and phase of

the 3D object at different planes by using a layered stereogram inverse Fresnel diffraction algorithm[3]. Compared with the 3D holographic fast Fourier transform algorithm that is rough in processing, the inverse Fresnel diffraction algorithm includes the accurate z-axis distance information of the different planes and, thus, can be employed to get the precise information of the 3D object through the diffraction between planes with distance. Based on this method, we define the complex amplitude of the 3D object as $U(x, y, z)$, and the complex amplitude distribution in the xy plane at the z position can be expressed by the Fresnel diffraction theory as

$$U(x,y)=\frac{\exp(jkz)}{j\lambda z}\exp\left[j\frac{k}{2z}(x^2+y^2)\right]\times F\left\{U(\xi,\eta)\exp\left[j\frac{k}{2z}(\xi^2+\eta^2)\right]\right\}, \tag{1}$$

where k is the wave vector, ξ and η are the spatial frequencies, and $F\{\}$ represents the Fourier transform. Then, the corresponding inverse Fresnel diffraction process would give the complex amplitude distribution in the xy plane of the hologram as

$$U(\xi,\eta)=\frac{j\lambda Z}{\exp(j\lambda z)}\exp\left[-j\frac{k}{2z}(\xi^2+\eta^2)\right]\times F^{-1}\left\{U(x,y)\exp\left[-j\frac{k}{2z}(x^2+y^2)\right]\right\}. \tag{2}$$

Next, we superpose all of the complex amplitude information at different planes and obtain the 3D complex amplitude distribution for the reconstruction. The amplitude and phase information of the complex amplitude distribution would be encoded into structure parameters and the position of the T-shaped nano-cavity in each unit cell, respectively, to form the meta-hologram structure. At last, under illumination of a linearly polarized light perpendicular to the slits, the desired 3D object can be reconstructed in free space.

To encode the amplitude information into the meta-hologram, we need to choose the appropriate structure parameters of the T-shaped nano-cavity. In Fig. 2, we study the influence of such structure parameters on the SPP's resonance, as well as the amplitude of transmitted light, based on the FDTD simulations. Figure 2(a) shows the amplitude transmittance through the T-shaped nano-cavity at 633 nm wavelength as a function of width w_2 and height h_2 of the lower cavity. The maximum transmittance is obtained at ($w_2 = 200$ nm, $h_2 = 50$ nm), which is about 4.2 times larger than the case of no lower cavity ($w_2 = w_1 = 50$ nm). In Figs. 2(b) and 2(d), we show the near-field electric-field distribution in the cavity for the two cases of suppressed and enhanced transmittance due to structure parameters, respectively. In Fig. 2(b), we can observe that the reflected field below the gold film is strong, and the transmitted light through the T-shaped nano-cavity is weak. In contrast, in Fig. 2(d), the reflected

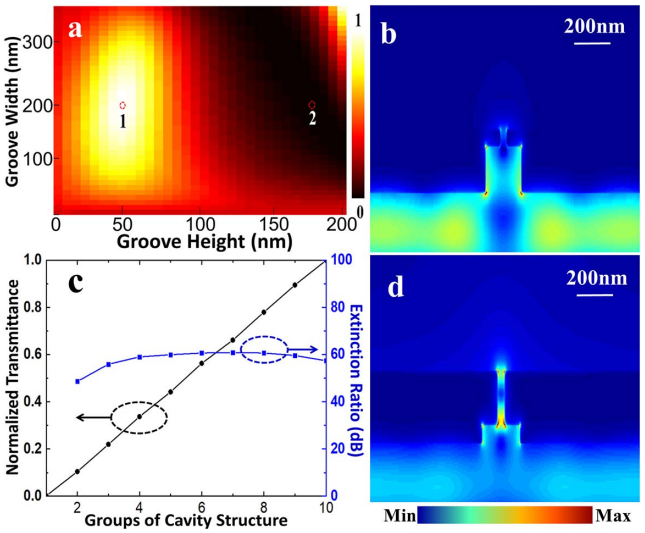

Fig. 2. a, Amplitude transmittance through the T-shaped nano-cavity at 633 nm wavelength as a function of the groove width w_2 and the groove height h_2. The other parameters are $P = 1$ μm, $H = 200$ nm, and $w_1 = 50$ nm. The two points at ($w_2 = 200$ nm, $h_2 = 180$ nm) and ($w_2 = 200$ nm, $h_2 = 50$ nm) indicate the two cases of suppressed and enhanced transmittance, whose near-field electric-field distributions are shown in b and d, respectively. c, Normalized transmittance (left) and polarization extinction ratio (right) as functions of 10 groups of cavity structure parameters ($h_2 = 50$ nm for all groups, $w_2 = 0$, 35, 50, 63, 72, 90, 105, 125, 150, 200 nm, respectively).

field is weak, and the electric field inside the slit is strong as well as the transmitted field on the top surface of gold film. We find that, in the T-shaped nano-cavity, SPPs are excited in the lower cavity due to light scattering, and the two side walls of the cavity could act as two reflecting mirrors to form SPP resonance inside the cavity. When the SPPs are controlled to be in a proper resonant state, more incident light energy can be coupled into the upper groove and greatly enhance the transmittance. The comparison between Figs. 2(b) and 2(d) proves that the transmittance can either be enhanced or suppressed by adjusting the cavity structure for amplitude modulation. Although the amplitude can be modulated continuously, as shown in Fig. 2(a), and provides better performance than the discrete modulation with limited steps, however, for the sake of reducing FDTD simulation time, we actually perform the amplitude modulation with 10 steps for the simulation of 3D object reconstruction. Figure 2(c) shows the 10-step amplitude transmittance based on 10 groups of cavity structure parameters (h_2, w_2) and the corresponding polarization extinction ratio. The amplitude transmittance is nearly linear with the 10 groups of (h_2, w_2); hence, they can be used for encoding the amplitude distribution to the meta-hologram. The polarization extinction ratio is defined as $10\log(T_p/T_s)$, where T_p and T_s are the transmittances for p- and s-polarized light. The values of the polarization extinction ratio for the 10 steps are all around 60 dB; hence, the meta-hologram would be excellent in polarization multiplexing. Note that in the 10 groups of

cavity structures, we choose constant h_2 and variable w_2, not only for the amplitude modulation, but also to maintain a large h_1 of the upper gold film for blocking directly transmitted light and keeping a high polarization extinction ratio.

In Fig. 3, we study the performance of the 3D object reconstruction with both amplitude and phase modulations. As an example shown in Fig. 3(a), two Chinese oracle characters ("sheep" and "rabbit") are designed to appear at two planes, $z_1 = 100$ μm and $z_2 = 120$ μm, respectively. To reconstruct such a pattern, we choose the meta-hologram with total size of 80 μm × 80 μm and each unit cell size of 1 μm × 1 μm, so the meta-hologram contains totally 80 × 80 unit cells. The amplitude and phase values of the 80 × 80 unit cells are presented in Figs. 3(b) and 3(c), respectively. Figures 3(d)–3(f) show the FDTD simulation results of the two oracle characters at the plane $z_2 = 120$ μm with three wavelengths of 633, 532, and 473 nm, respectively. It is observed that, for all wavelengths, the oracle "rabbit" is always clear, just as our design, while the oracle "sheep" is always blurry due to the defocus status. In contrast, the opposite results are presented at the plane of $z_1 = 100$ μm in Figs. 3(g)–3(i), where the "sheep" is clear and the "rabbit" is fuzzy, well agreeing with the design in Fig. 3(a). For the three different wavelengths, the reconstruction results are almost the same, demonstrating the broadband response property of the meta-hologram. According to the formula $\theta = \arcsin(\lambda/P)$, the holographic pattern appears at three different output angles of 39.27°, 32.14°, and 28.23° for the wavelengths of 633, 532, and 473 nm, respectively, which indicates that the structure could be employed to realize 3D color holography[26,31–34]. The efficiency (energy of the desired pattern over the total transmitted energy) of the meta-hologram is about 29.7%, and the total light transmittance through the meta-hologram is about 11% at 633 nm due to the high reflection and absorption of gold film.

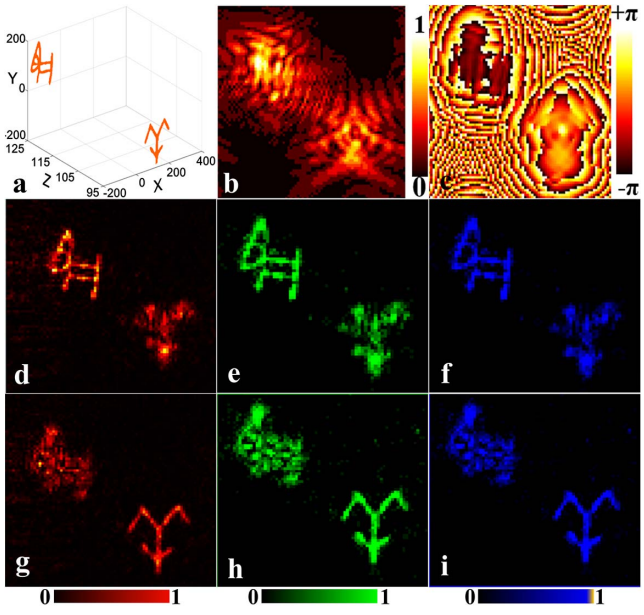

Fig. 3. a, Original 3D object comprises two Chinese oracle characters ("sheep" and "rabbit") located at two planes, $z_1 = 100$ μm and $z_2 = 120$ μm, respectively. b, The 10-step quantized amplitude distribution in the hologram recording plane. c, The corresponding continuous phase distribution. d–f, Reconstructed images at 633, 532, and 473 nm wavelength in the plane $z_2 = 120$ μm, respectively. g–i, Reconstructed images at 633, 532, and 473 nm wavelength in the plane $z_1 = 100$ μm, respectively.

To further demonstrate the superiority of the proposed meta-hologram with both amplitude and phase control, we compare it to the case of the phase-only meta-hologram with uniform amplitude ($w_2 = w_1 = 50$ nm), as shown in Fig. 4. In Fig. 4(a), we design a 3D object including three letters ("N", "R", "C") located at three planes $z_3 = 100$ μm, $z_2 = 80$ μm, and $z_1 = 60$ μm, respectively. Here, we still choose 80 × 80 unit cells to build the meta-hologram, and all parameters are the same as in Fig. 3. Figures 4(b)–4(d) show the FDTD simulation results of the three letters at the three planes with both amplitude and phase modulation. It can be seen that the letters "N", "R", "C" become clear at the three planes, respectively, demonstrating good reconstruction for the original design in Fig. 4(a). In contrast, Figures 4(e)–4(g) show the reconstruction of the three letters based on the phase-only meta-hologram. We find that, although the three letters "N", "R", "C" appear at the desired planes, respectively, the generated letters are not as clear as the compared one, and the speckle noise is stronger, similar to the previous report[24]. The SNR, defined as the ratio of the maximum intensity in the holographic image to the standard deviation of the background noise[24], is used to quantitatively evaluate the image quality. For the reconstructed image in Fig. 4(b), the SNR is 57.6 with the background area of 25 μm × 25 μm, while in Fig. 4(e) the SNR is 39.7 with worse image quality. We also tried the parameters ($w_2 = 200$ nm, $h_2 = 50$ nm) with maximum transmittance for the phase-only case and found that the SNR

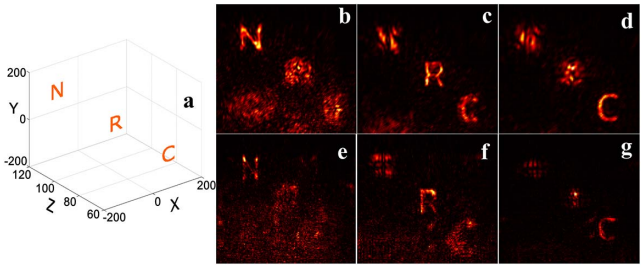

Fig. 4. a, Original 3D object comprises three letters ("N", "R", "C") located at three planes $z_3 = 100$ μm, $z_2 = 80$ μm, $z_1 = 60$ μm, respectively. b–d, Reconstructed images at 633 nm wavelength in the three planes (z_3, z_2, z_1), respectively, based on the meta-hologram with complex amplitude modulation. e–g, Reconstructed images at 633 nm wavelength in the three planes (z_3, z_2, z_1), respectively, based on the phase-only meta-hologram.

is almost the same. For the two-/four-level amplitude modulation cases, the SNR is calculated as 40.3 and 45.4, respectively, which is also worse than the 10-level case [Fig. 4(b)]. Such comparisons prove that the meta-hologram with complex amplitude modulation can effectively suppress speckle noise, unlike the phase-only case, and provide better image quality in 3D object reconstruction.

In conclusion, we propose and study a new plasmonic meta-hologram based on a T-shaped nano-cavity and detour phase and achieve simultaneous amplitude and phase control for 3D holographic imaging. Due to the SPP's resonance in the T-shaped nano-cavity, the transmission amplitude can either be enhanced or suppressed by adjusting the cavity structure parameters, thus contributing to continuous amplitude modulation. While the phase modulation of 0–2π can be realized by changing the position of the T-shaped nano-cavity in each unit cell according to the detour phase principle, we numerically demonstrate that the meta-hologram can be employed to reconstruct 3D objects in a broadband wavelength range including 633, 532, and 473 nm. We also prove that such a device with complex amplitude modulation could suppress speckle noise and get better image quality compared to the phase-only meta-hologram.

Finally, although here we study the meta-hologram numerically, such a T-shaped nano-cavity can be fabricated according to previous experimental study[35], where the focused ion beam technique was used to fabricate the SPP cavities of variable widths and then the nano-slit through the gold film in the middle of each cavity. Because the detour phase used here is only dependent on the position of nano-scatterer in each unit cell, such a device could be merged with other phase modulation methods, depending on orientation or structure of the nano-scatterer (e.g., propagation phase or geometric phase) to promise a more flexible hologram[36,37]. Due to the limited 80×80 unit cells, here, the demonstrated hologram quality is worse than previous reports[5,24,28]; hence, the number of unit cells can be increased to enhance the performance with more accurate complex amplitude values. The proposed meta-hologram device could offer great potential in various applications, such as 3D displays, complex laser-beam shaping, optical communications, and others.

This work was supported by the National Natural Science Foundation of China (Nos. 61427819, 91750205, 61490712, U1701661, and 61605117), the National Key Basic Research Program of China (973) (No. 2015CB352004), the Leading Talents of Guangdong Province Program (No. 00201505), the Natural Science Foundation of Guangdong Province (Nos. 2016A030312010, 2016A030310063, and 2017A030313351), and the Science and Technology Innovation Commission of Shenzhen (Nos. KQTD2017033011044403, ZDSYS201703031605029, and JCYJ2017818144338999).

References

1. D. Gabor, Nature **161**, 777 (1948).
2. P. Hariharan, *Optical Holography: Principles, Techniques and Applications* (Cambridge University, 1996).
3. T. C. Poon, *Digital Holography and Three-Dimensional Display* (Springer, 2006).
4. P. Genevet and F. Capasso, Rep. Prog. Phys. **78**, 024401 (2015).
5. G. X. Zheng, H. Mühlenbernd, M. Kenney, G. X. Li, T. Zentgraf, and S. Zhang, Nat. Nanotechnol. **10**, 308 (2015).
6. L. Zhang, S. Mei, K. Huang, and C. W. Qiu, Adv. Opt. Mater. **4**, 818 (2016).
7. S. Sun, Q. He, S. Xiao, Q. Xu, X. Li, and L. Zhou, Nat. Mater. **11**, 426 (2012).
8. L. Huang, X. Chen, H. Mühlenbernd, G. Li, B. Bai, Q. Tan, G. Jin, T. Zentgraf, and S. Zhang, Nano Lett. **12**, 5750 (2012).
9. S. Sun, K.-Y. Yang, C.-M. Wang, T.-K. Juan, W. Chen, C. Liao, Q. He, S. Xiao, W.-T. Kung, G.-Y. Guo, L. Zhou, and D. Tsai, Nano Lett. **12**, 6223 (2012).
10. A. V. Kildishev, A. Boltasseva, and V. M. Shalaev, Science **339**, 1232009 (2013).
11. D. Wen, F. Yue, G. Li, G. Zheng, K. Chan, S. Chen, M. Chen, K. F. Li, P. W. H. Wong, K. W. Cheah, E. Y. B. Pun, S. Zhang, and X. Chen, Nat. Commun. **6**, 8241 (2015).
12. N. Yu, P. Genevet, M. A. Kats, F. Aieta, J. P. Tetienne, F. Capasso, and Z. Gaburro, Science **334**, 333 (2011).
13. Q. Xu, X. Zhang, Y. Xu, C. Ouyang, Y. Li, J. Han, and W. Zhang, Chin. Opt. Lett. **16**, 050002 (2018).
14. M. Khorasaninejad, W. T. Chen, R. C. Devlin, J. Oh, A. Y. Zhu, and F. Capasso, Science **352**, 1190 (2016).
15. S. Wang, P. C. Wu, V.-C. Su, Y.-C. Lai, C. H. Chu, J.-W. Chen, S.-H. Lu, J. Chen, B. Xu, C.-H. Kuan, T. Li, S. Zhu, and D. P. Tsai, Nat. Commun. **8**, 187 (2017).
16. M. Pu, X. Li, X. Ma, Y. Wang, Z. Zhao, C. Wang, C. Hu, P. Gao, C. Huang, H. Ren, X. Li, F. Qin, J. Yang, M. Gu, M. Hong, and X. Luo, Sci. Adv. **1**, e1500396 (2015).
17. R. M. Kerber, J. M. Fitzgerald, D. E. Reiter, S. Oh, and O. Hess, ACS Photon. **4**, 891 (2017).
18. J. Wang, Chin. Opt. Lett. **16**, 050006 (2018).
19. X. Yin, Z. Ye, J. Rho, Y. Wang, and X. Zhang, Science **339**, 1405 (2013).
20. C. Choi, S.-J. Kim, J.-G. Yun, J. Sung, S.-Y. Le, and B. Lee, Chin. Opt. Lett. **16**, 050009 (2018).
21. E. Maguid, I. Yulevich, D. Veksler, V. Kleiner, M. L. Brongersma, and E. Hasman, Science **352**, 1202 (2016).
22. M. Khorasaninejad, A. Ambrosio, P. Kanhaiya, and F. Capasso, Sci. Adv. **2**, e1501258 (2016).
23. L. Huang, X. Chen, H. Mühlenbernd, H. Zhang, S. Chen, B. Bai, Q. Tan, G. Jin, K.-W. Cheah, C.-W. Qiu, J. Li, T. Zentgraf, and S. Zhang, Nat. Commun. **4**, 2808 (2013).
24. G.-Y. Lee, G. Yoon, S.-Y. Lee, H. Yun, J. Cho, K. Lee, H. Kim, J. Rho, and B. Lee, Nanoscale **10**, 4237 (2018).
25. X. Ni, A. V. Kildishev, and V. M. Shalaev, Nat. Commun. **4**, 2807 (2013).
26. W. Wan, J. Gao, and X. Yang, ACS Nano **10**, 10671 (2016).
27. C. J. Min, J. P. Liu, T. Lei, G. Y. Si, Z. W. Xie, J. Lin, L. P. Du, and X. C. Yuan, Laser Photon. Rev. **10**, 978 (2016).
28. Z. W. Xie, T. Lei, G. Y. Si, X. Y. Wang, J. Lin, C. J. Min, and X.-C. Yuan, ACS Photon. **4**, 2158 (2017).
29. B. R. Brown and A. W. Lohmann, Appl. Opt. **5**, 967 (1966).
30. A. W. Lohmann and D. P. Paris, Appl. Opt. **6**, 1739 (1967).
31. Y. Montelongo, J. O. Tenorio-Pearl, C. Williams, S. Zhang, W. I. Milne, and T. D. Wilkinson, Proc. Natl. Acad. Sci. USA **111**, 12679 (2014).

32. X. Li, L. Chen, Y. Li, X. Zhang, M. Pu, Z. Zhao, X. Ma, Y. Wang, M. Hong, and X. Luo, Sci. Adv. **2**, e1601102 (2016).
33. X. Zhang, M. Pu, J. Jin, X. Li, P. Gao, X. Ma, C. Wang, and X. Luo, Annalen der Physik **529**, 1700248 (2017).
34. Y.-W. Huang, W. T. Chen, W.-Y. Tsai, P. C. Wu, C.-M. Wang, G. Sun, and D. P. Tsai, Nano Lett. **15**, 3122 (2015).
35. Q. Min and R. Gordon, Opt. Express **16**, 9708 (2008).
36. Y. Guo, M. Pu, Z. Zhao, Y. Wang, J. Jin, P. Gao, X. Li, X. Ma, and X. Luo, ACS Photon. **3**, 2022 (2016).
37. F. Zhang, M. Pu, J. Luo, H. Yu, and X. Luo, Opto-Electron. Eng. **44**, 319 (2017).